

Experimental realization of deterministic and selective photon addition in a bosonic mode assisted by an ancillary qubit

Downloaded from: https://research.chalmers.se, 2025-10-16 09:28 UTC

Citation for the original published paper (version of record):

Kudra, M., Jirlow, M., Kervinen, M. et al (2025). Experimental realization of deterministic and selective photon addition in a bosonic mode assisted by an ancillary qubit. QUANTUM SCIENCE AND TECHNOLOGY, 10(4). http://dx.doi.org/10.1088/2058-9565/ae0519

N.B. When citing this work, cite the original published paper.

research.chalmers.se offers the possibility of retrieving research publications produced at Chalmers University of Technology. It covers all kind of research output: articles, dissertations, conference papers, reports etc. since 2004. research.chalmers.se is administrated and maintained by Chalmers Library







PAPER • OPEN ACCESS

Experimental realization of deterministic and selective photon addition in a bosonic mode assisted by an ancillary qubit

To cite this article: Marina Kudra et al 2025 Quantum Sci. Technol. 10 045037

View the article online for updates and enhancements.

You may also like

- A simple protocol for fault tolerant verification of quantum computation
 Alexandru Gheorghiu, Matty J Hoban and Elham Kashefi
- <u>Typical machine learning datasets as low-depth quantum circuits</u>
 Florian J Kiwit, Bernhard Jobst, Andre Luckow et al.
- Electro-optic sampling of the electric-field operator for ultrabroadband pulses of Gaussian quantum light Geehyun Yang, Sandeep Sharma and Andrey S Moskalenko



Quantum Science and Technology



OPEN ACCESS

RECEIVED

2 May 2025

REVISED

19 August 2025

ACCEPTED FOR PUBLICATION

9 September 2025

PUBLISHED

18 September 2025

Original Content from this work may be used under the terms of the Creative Commons Attribution 4.0 licence.

Any further distribution of this work must maintain attribution to the author(s) and the title of the work, journal citation and DOI.



PAPER

Experimental realization of deterministic and selective photon addition in a bosonic mode assisted by an ancillary qubit

Marina Kudra¹, Martin Jirlow¹, Mikael Kervinen¹, Axel M Eriksson¹, Fernando Quijandría², Per Delsing¹, Tahereh Abad^{1,*} and Simone Gasparinetti^{1,*}

- Department of Microtechnology and Nanoscience, Chalmers University of Technology, 412 96 Gothenburg, Sweden
- Quantum Machines Unit, Okinawa Institute of Science and Technology Graduate University, Onna-son, Okinawa 904-0495, Japan
- * Authors to whom any correspondence should be addressed.

E-mail: tahereh.abad@chalmers.se and simoneg@chalmers.se

Keywords: bosonic codes, circuit QED, quantum error correction, quantum information processing, microwave cavities, parity recovery by single-photon addition

Supplementary material for this article is available online

Abstract

Bosonic quantum error correcting codes are primarily designed to protect against single-photon loss. To correct for this type of error, one can encode the logical qubit in code spaces with a definite photon parity, such as cat codes or binomial codes. Error correction requires a recovery operation that maps the error states—which have opposite parity—back onto the code space. Here, we realize a collection of photon-number-selective, simultaneous photon addition operations on a bosonic mode, a microwave cavity, assisted by a superconducting qubit. These operations are implemented as two-photon transitions that excite the cavity and the qubit at the same time. The additional degree of freedom of the qubit makes it possible to implement a coherent, unidirectional mapping between spaces of opposite photon parity. We present the successful experimental implementation of the drives and the phase control they enable on superpositions of Fock states. The presented technique, when supplemented with qubit reset, is suitable for autonomous quantum error correction in bosonic systems and, more generally, opens the possibility to realize a range of non-unitary transformations on a bosonic mode.

1. Introduction

Encoding quantum information in bosonic modes, such as harmonic oscillators, is a promising platform for error correctable quantum computing [1]. However, in order to control the quantum information in a linear mode beyond Gaussian operations, some nonlinearity is required, which is commonly realized by an ancilla qubit dispersively coupled to the bosonic mode. The dispersive interaction enables an indirect control of the oscillator states and allows for different gates to be implemented. Examples are the selective number-dependent arbitrary phase (SNAP) gate [2–4] that changes only the phases of the Fock states, echoed conditional displacement [5] that generates conditional displacements in phase-space, and optimal control pulses [6] that in general can change both the phases and the populations of the bosonic mode.

Precise control of the bosonic mode enables quantum error correction against unwanted or uncontrolled errors [7]. Often, the dominant source of error in a bosonic mode is single-photon loss. Bosonic codes such as the cat and binomial codes remain invariant under discrete-order rotations in phase space. The order of such a rotation determines their Fock space structure and, consequently, their robustness against photon loss and gain errors. For instance, the four-component cat code [8], i.e. a superposition of four orthogonal coherent states, is the smallest-order version of the cat code which is robust against single-photon losses [9]. The logical words of the cat code are parity eigenstates and therefore by periodically monitoring the parity of the system we find whether an error has happened or not. Ofek et.al. [10] successfully implemented the real-time parity detection of cat codes and subsequent active reset of the qubit, but they did not correct the deterministic loss of amplitude of the cat states. Another approach is to use the binomial code [11, 12] and

after parity detection use optimal control pulses synthesized by GRAPE [6] to go back to the code space. An alternative to the above protocols corresponds to the recently introduced parity recovery by selective photon addition (PReSPA) [13]. This is an autonomous, measurement-free error correction scheme realized by means of number-selective continuous wave driving fields. PReSPA is implemented by driving two sets of microwave combs, both of which have to be photon-number selective. This is a disadvantage as it restricts the rates of all the drives. If we were to implement PReSPA in a pulsed version, both pulses would have to be long compared to the inverse of the dispersive shift. We propose to implement the same autonomous recovery of parity by applying a selective number-dependent arbitrary-phase photon-addition (SNAPPA) gate followed by a fast unconditional qubit reset.

The SNAPPA gate is described by

$$S_{\text{PA}}\left(\left\{ (\theta_i)_{n_i \to n_{i+1}} \right\} \right) \equiv \sum_{i \subset N} e^{i\theta_i} |n_i + 1\rangle |e\rangle \langle n_i |\langle g| + \text{h.c.},$$
(1)

where $|n_i\rangle$ are the Fock states which are affected by the transformation when the qubit is in the ground state, $\{\theta_i\}$ are the corresponding phases they acquire, and $|g\rangle$ and $|e\rangle$ are the ground and excited states of the qubit, respectively. We implement this gate by driving a two-photon transition of the combined qubit-cavity system. We show that we can selectively add photons to the odd-parity subspace without affecting the even-parity subspace. Moreover, we control the relative phases of the added photons by adjusting the phases of the off-resonant drives. The two-photon transition $|0\rangle|g\rangle \rightarrow |1\rangle|e\rangle$ was previously implemented in order to create entanglement between two distant transmon qubits [14]. A special case of the SNAPPA gate, where the transitions for all Fock states $|n\rangle$ are driven simultaneously and $\theta_n=0$ for all n corresponds to the so-called 'conventional' single-photon addition on the bosonic mode, which was implemented in trapped ions [15]. The latter operation is not to be confused with the bosonic ladder operator \hat{a}^{\dagger} [16].

2. Methods

We implement SNAPPA in a circuit quantum electrodynamics setup comprising a long-lived microwave cavity [17, 18], a dispersively coupled transmon qubit, and a readout resonator. We cool down the device, which is similar to reference [4], in a dilution refrigerator with a base temperature below 10 mK. We control the whole system with a single microwave transceiver that uses direct digital synthesis to generate microwave pulses up to 8.5 GHz with an instantaneous bandwidth of 1 GHz [19].

The relevant part of the qubit-cavity system is described by the Hamiltonian [2]

$$H = \omega_c a^{\dagger} a - \frac{K_c}{2} a^{\dagger 2} a^2 + \omega_q q^{\dagger} q - \frac{\alpha_q}{2} q^{\dagger 2} q^2 - \chi a^{\dagger} a q^{\dagger} q - \frac{\chi'}{2} a^{\dagger 2} a^2 q^{\dagger} q, \tag{2}$$

where ω_c and ω_q are the resonance frequencies of the cavity and the transmon qubit, K_c is the Kerr nonlinearity of the cavity, α_q is the qubit anharmonicity, χ is the dispersive shift between the cavity and the qubit, χ' is a photon-number-dependent correction to the dispersive shift, a^{\dagger} (a) is the creation (annihilation) operator of the cavity field and similarly, and q^{\dagger} (q) is the raising (lowering) operator of the qubit. The Hamiltonian parameters and the coherence properties of the system are listed in [20].

We implement SNAPPA by applying off-resonant drives to the qubit and the cavity, whose frequencies sum up to implement the two-excitation transitions $|n\rangle|g\rangle$ to $|n+1\rangle|e\rangle$ at frequencies $\omega_c + \omega_q - (n+1)\chi$. We apply one qubit drive at frequency $\omega_q - \Delta$, where Δ is detuning between the qubit transition frequency and the drive frequency and a frequency comb to the cavity at frequencies $\{\omega_c + \Delta - (n_i + 1)\chi\}$, with one component for each transition $|n_i\rangle|g\rangle$ to $|n_i + 1\rangle|e\rangle$. Which states $\{n_i\}$ are addressed is chosen by applying the appropriate frequency of the cavity frequency comb. The phase θ_i that will be added to the final Fock state $|n_i + 1\rangle$ is determined by the relative phases of the drive at the frequency $\omega_c + \Delta - (n_i + 1)\chi$. The level diagram in figure 1 illustrates the SNAPPA gate $S_{\text{PA}}(\theta_{1 \to 2}, \theta_{3 \to 4}, \theta_{5 \to 6})$, which requires one frequency tone to the qubit (green arrows) and three tones to the cavity (in shades of magenta arrows).

When choosing Δ , the condition $|\Delta - (n_{\max} + 1)\chi| \gg 1/\tau$ (where τ is the gate time) has to hold, so that the pulses we send are not driving cavity displacements or qubit rotations directly. In our experiments we simultaneously address up to 3 transitions with a maximum Fock number of 5. On the other hand, Δ should be smaller than qubit anharmonicity $|\alpha_b|$ to avoid driving the first-to-second-excited-state qubit transition. A smaller Δ is also preferable to achieve the same effective strength with less power in the driving tones. In principle, driving the qubit at the frequency $\omega_q + \Delta$ should avoid this restriction. Nevertheless, our experimental attempts did not yield the desired results. Based on an analysis of the effective Hamiltonian [21], we suspect the presence of a destructive interference effect arising from Stark shifts. The pulses have to be selective depending on the Fock number in the cavity, thus we require $\tau \gg 1/\chi$. At the

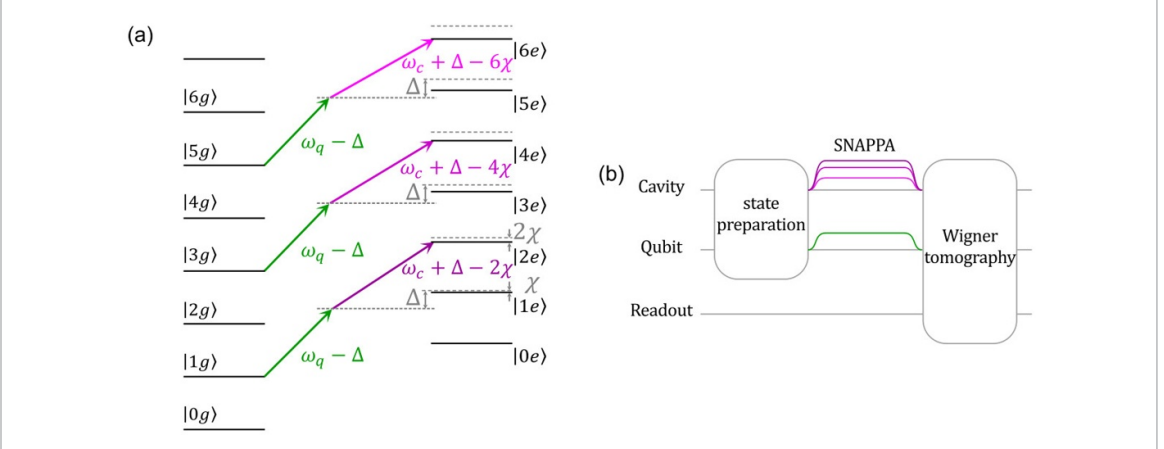


Figure 1. (a) Level diagram sketching the SNAPPA gate, here implemented to map the cavity odd parity subspace onto the even-parity subspace, without compromising the even-parity states. The qubit off-resonant drive at frequency $\omega_q - \Delta$ is common for all the transitions(green arrows). In different shades of magenta arrows, the cavity off-resonant drives at frequencies $\omega_c + \Delta - (n+1)\chi$ enable the transition from $|n\rangle|g\rangle$ to $\mathrm{e}^{\mathrm{i}\theta_n}|n+1\rangle|e\rangle$, for each odd n respectively. The phase θ_n is directly related to the relative phases of the drives $\omega_c + \Delta - (n+1)\chi$ (b) Pulse sequence used to apply the SNAPPA gate. We initialize the cavity and the qubit to $|\Psi\rangle|g\rangle$, apply the SNAPPA gate, and perform direct Wigner tomography to measure the state of the cavity.

same time, τ should be chosen as short as possible to avoid qubit dephasing and decoherence during the operation. Based on these tradeoffs, we choose pulses with length of $\tau = 4.2 \,\mu s$ with a 100 ns sin² rise- and fall-time for $n_{\rm max} = 5$, $\chi = 1.4 \, {\rm MHz}$, and $\Delta/(2\pi) = 30 \, {\rm MHz}$.

The off-resonant drives induce Stark shifts of both the qubit and the cavity frequencies and hence the two-excitation transitions require a frequency correction $d\omega_n$, which we include in the cavity off-resonant drives $\omega_c + \Delta - (n+1)\chi + d\omega_n$, where $d\omega_n/(2\pi)$ is of the order of a few hundred kHz and is calibrated together with the amplitudes and phases of all the drives in the self-consistent procedure we explain in [20].

To characterize SNAPPA, we initially prepare a range of non-classical states using a sequence of three displacements and two optimized SNAP gates [4]. After the gate, we perform direct Wigner tomography of the cavity mode [2], where we apply a displacement of varying complex amplitude α followed by a Ramsey measurement at a fixed time delay of $1/(2\chi) \approx 360$ ns, which returns the photon parity of the cavity mode as the outcome of the qubit measurement. The Wigner function is obtained as

$$W(\alpha) = \frac{2}{\pi} \text{Tr} \left[D^{\dagger}(\alpha) \rho D(\alpha) \Pi \right], \tag{3}$$

where Π is the parity operator. We reconstruct the density matrix of the target state from the Wigner function using a recently developed neural-network-based approach [22, 23] which reconstructs the density matrix of the state by minimizing a cost function between the reconstructed state and the measured Wigner tomography data.

3. Results

3.1. Using SNAPPA to recover parity with controllable relative phase

For logical states with a fixed parity, single-photon loss projects the states into the orthogonal parity subspace. Thus, we use two-excitation selective transitions to project the states back into the logical states. The two-excitation selective transitions have to map the phase of odd Fock states (error) to their even counterparts (computational) and excite the qubit. At the same time, they should keep the even-parity subspace unchanged and leave the qubit in the ground state.

We evaluate these requirements by preparing $(|1\rangle+|3\rangle)|g\rangle/\sqrt{2}$ and $(|2\rangle+|4\rangle)|g\rangle/\sqrt{2}$ shown in figures 2(a) and (e), respectively. We apply the SNAPPA gate $S_{\text{PA}}(0_{1\to2},\theta_{3\to4})$ for $\theta_{3\to4}=0,\pi,-\pi/2$ by applying a qubit off-resonant drive at frequency $\omega_q-\Delta$ and two cavity off-resonant drives at frequencies $\omega_c+\Delta-2\chi$ and $\omega_c+\Delta-4\chi$ in order to drive transitions $|1\rangle|g\rangle\to|2\rangle|e\rangle$ and $|3\rangle|g\rangle\to|4\rangle|e\rangle$ simultaneously. We then vary the phase of the second cavity drive at frequency $\omega_c+\Delta-4\chi$ to vary the phase $\theta_{3\to4}$.

Qubit population and fidelity of the cavity state are listed in table 1. Because we perform Wigner tomography directly after applying the state preparation gates and the SNAPPA gates, the reported fidelities suffer from different type of errors due to residual qubit population and qubit-cavity entanglement. We measure an average excited state population of the qubit of about 5% after preparing the initial states. We

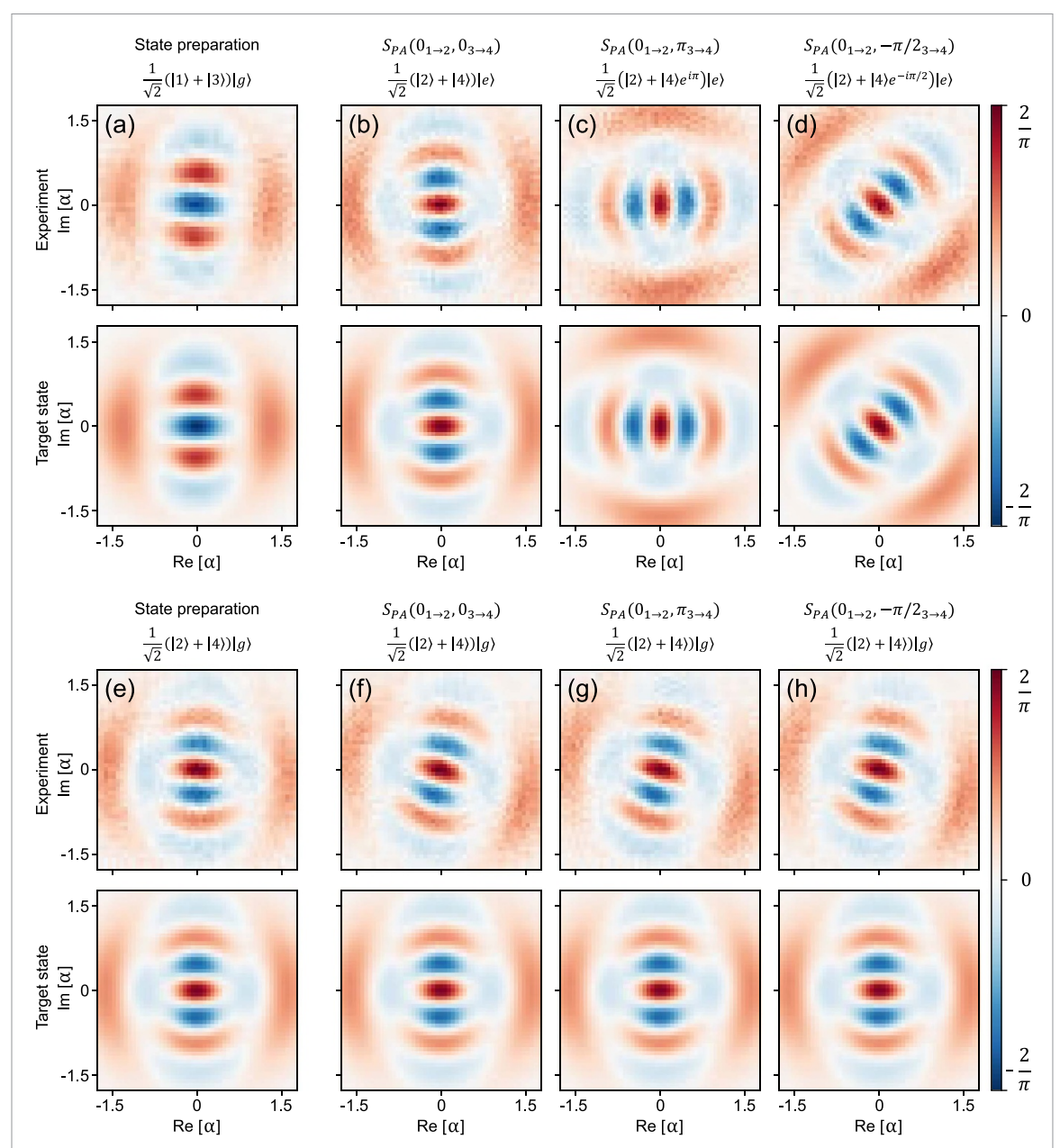


Figure 2. Characterization of the SNAPPA gate $S_{PA}(0_{1\rightarrow2},\theta_{3\rightarrow4})$ to map odd-parity states, i.e. $\{|1\rangle,|3\rangle\}$ to even-parity states, i.e. $\{|2\rangle,|4\rangle\}$, while the even states are almost unaffected by the SNAPPA gate. Wigner functions of experimental versus target states when the SNAPPA gate is applied to (a)–(d) an error initial state and (e)–(h) a computational initial state. (a) Initial state $(|1\rangle+|3\rangle)|g\rangle/\sqrt{2}$ and final/target states $(|2\rangle+|4\rangle e^{i\theta_3\rightarrow 4})|e\rangle/\sqrt{2}$, where $\theta_{3\rightarrow 4}$ is the phase of the cavity off-resonant drive $\omega_c+\Delta-4\chi$, given by (b) $\theta_{3\rightarrow 4}=0$, (c) $\theta_{3\rightarrow 4}=\pi$, (d) $\theta_{3\rightarrow 4}=\pi/2$. The lower panels show that the drives have little to no effect on the even-parity subspace. (e) Initial state $(|2\rangle+|4\rangle)|g\rangle/\sqrt{2}$ and (f)–(h) identical final state $(|2\rangle+|4\rangle)|g\rangle/\sqrt{2}$ for $\theta_{3\rightarrow 4}=0$, $\pi,-\pi/2$.

also observe a reduced contrast in the Ramsey sequence used for Wigner tomography, corresponding to an additional 3 to 4% change in qubit population, due to the SNAPPA gate. Resetting the qubit prior to the tomography step would lead to a more accurate estimate of the fidelity. In [20], we show that any initial population in the qubit leads to a direct misassignment of the measured photon-number parity, with the error probability equal to the initial qubit excitation. This highlights the importance of qubit reset before tomography to ensure an accurate reconstruction of the Wigner function, which we leave for future work.

We analyze the error budget of the SNAPPA gate by numerically simulating the transitions $|1\rangle|g$ $\rangle \to |2\rangle|e\rangle$ and $|3\rangle|g\rangle \to |4\rangle|e\rangle$ simultaneously, both with and without decoherence error channels. Additionally, we simulate the system with incoherent errors only in either the qubit or cavity, respectively, to assess the error contributions from each component. The drive parameters are numerically optimized to maximize the fidelity of the target state. The fidelity of the simulated bosonic state is calculated by tracing out the qubit and determining the overlap with the target state.

Table 1. Qubit population and fidelity to target state. Fidelities marked with * are fidelities to the rotated state $(|2\rangle + |4\rangle e^{i0.53})|g\rangle/\sqrt{2}$.

Figure	Target state	Qubit population	Fidelity bosonic state
2(a)	$1/\sqrt{2}(1\rangle+ 3\rangle) g\rangle$	0.04	0.96
2 (b)	$1/\sqrt{2}(2\rangle+ 4\rangle) e\rangle$	0.92	0.94
2 (c)	$1/\sqrt{2}(2\rangle + 4\rangle e^{i\pi}) e\rangle$	_	0.93
2(d)	$1/\sqrt{2}(2\rangle + 4\rangle e^{-i\pi/2}) e\rangle$	_	0.94
2 (e)	$1/\sqrt{2}(2\rangle + 4\rangle) g\rangle$	0.06	0.93
2(f)	$1/\sqrt{2}(2\rangle + 4\rangle) g\rangle$	0.09	0.92^{*}
2(g)	$1/\sqrt{2}(2\rangle + 4\rangle) g\rangle$	_	0.93*
2(h)	$1/\sqrt{2}(2\rangle + 4\rangle) g\rangle$	_	0.92^{*}
3(a)	$1/\sqrt{3}(1\rangle+ 3\rangle+ 5\rangle) g\rangle$	0.05	0.92
3(b)	$1/\sqrt{3}(2\rangle+ 4\rangle+ 6\rangle) e\rangle$	0.90	0.93
3(c)	$1/\sqrt{3}(2\rangle + 4\rangle e^{i\pi} + 6\rangle) e\rangle$	_	0.93
3(d)	$1/\sqrt{3}(2\rangle + 4\rangle + 6\rangle e^{i\pi}) e\rangle$	_	0.93
3(e)	$1/\sqrt{3}(2\rangle + 4\rangle e^{i\pi} + 6\rangle e^{i\pi}) e\rangle$	_	0.93
4 (a)	$1/\sqrt{2}(0\rangle+ 1\rangle e^{i\pi}) g\rangle$	0.02	0.93
4 (b)	$1/\sqrt{2}(1\rangle+ 2\rangle e^{\mathrm{i}\pi}) e\rangle$	0.94	0.92
4 (c)	$(\sqrt{2}/\sqrt{3} 1\rangle + 1/\sqrt{3} 3\rangle) g\rangle$	0.05	0.90
4 (d)	$(\sqrt{2}/\sqrt{3} 2\rangle + 1/\sqrt{4} 3\rangle) e\rangle$	0.91	0.96

Table 2. Simulated error budget for the transition $\frac{1}{\sqrt{2}}(|1\rangle+|3\rangle)|g\rangle \rightarrow \frac{1}{\sqrt{2}}(|2\rangle+|4\rangle)|e\rangle$, with and without decoherence.

Included error	Qubit population	Fidelity bosonic state
No error	0.98	0.97
Qubit relaxation	0.88	0.87
Cavity relaxation	0.96	0.94
Both qubit & cavity	0.87	0.85

The simulated qubit populations and cavity state fidelities are presented in table 2. The results indicate that qubit decoherence is the dominant incoherent error. The drive parameters used in the simulation were optimized assuming the absence of losses, which explains the larger infidelities observed here compared to the experimental results presented in table 1.

Note that while coherent errors due to entanglement also exist, table 2 indicates that the qubit relaxation is the dominant contribution.

Abrupt transition to the phase of the second cavity drive, we directly change the phase of the Fock state $|4\rangle$ for the odd-parity initial state (figures 2(b)–(d)). The fidelity is 0.02-0.03 lower than the state preparation fidelity. The observed reduction in fidelity following the application of SNAPPA can likely be attributed to two factors. First, during SNAPPA drives, the injection of photons into the cavity will increase its susceptibility to loss errors. Second, fidelity diminishes during Wigner tomography when the qubit starts in its excited state, as it is more susceptible to decoherence.

As seen in table 1, particularly after applying the SNAPPA gate, the qubit error is larger than the cavity error for transitions that excite the qubit due to the stronger decay rate of the qubit. As mentioned above, the dominant source of error in SNAPPA is qubit relaxation. During the gate operation, transitions such as $(|1\rangle + |3\rangle)|g\rangle/\sqrt{2}$ to $(|2\rangle + |4\rangle)|e\rangle/\sqrt{2}$, shown in table 1 2(b), are driven by tuning the drive parameters to induce Rabi oscillations. At the point of full transition, which we set to occur at 4.2 μ s, a single photon is already being injected into the cavity, and the qubit is expected to be in its excited state. If the qubit decays during this period, the resulting incoherent errors primarily affect the qubit population rather than the cavity photon number, leading to a higher error rate for the transmon. So the transmon is expected to experience greater error than the cavity.

For the even-parity initial state, the outcome remains unchanged with the change of the phase (figures 2(f)–(h)), except for the rotation of all the states by 0.53 ± 0.03 rad that is found by maximizing the fidelity to the $(1/\sqrt{2})(|2\rangle+|4\rangle)$ state. Part of the rotation, 0.25 rad, can be attributed to cavity Kerr evolution during the two-photon drive. The remaining rotation likely results from other contributions to the Hamiltonian, such as Stark shifts induced by the drives and drive-dependent higher-order Kerr effects. The code words undergo a deterministic rotation under the action of the error-correcting drives, which can be

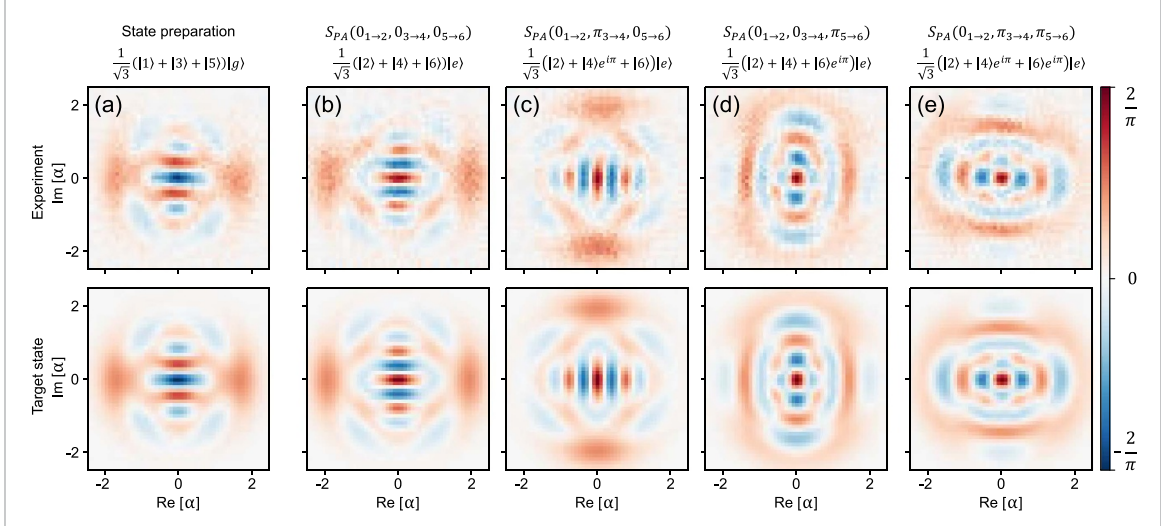


Figure 3. Wigner functions of experimentally obtained and target states when SNAPPA gate $S_{\text{PA}}(0_{1\rightarrow2},\theta_{3\rightarrow4},\theta_{5\rightarrow6})$ is applied. (a) Initial state $1/\sqrt{3}(|1\rangle+|3\rangle+|5\rangle)|g\rangle$ and the resulting states after one iteration of applying the drives $(|2\rangle+|4\rangle e^{i\theta_{3\rightarrow4}}+|6\rangle e^{i\theta_{5\rightarrow6}})|e\rangle/\sqrt{3}$, where $(\theta_{3\rightarrow4},\theta_{5\rightarrow6})$ is the phase of cavity off-resonant drive with frequency $\omega_c+\Delta-4\chi$ and $\omega_c+\Delta-6\chi$, respectively, given by (b) (0,0), (c) $(\pi,0)$, (d) $(0,\pi)$ and (e) (π,π) .

compensated for by rotating the cavity states (or updating the reference frame of the cavity drive), conditioned on the outcome of the qubit measurement.

3.2. Scaling SNAPPA

It is important to be able to drive more transitions without significantly impacting the fidelity of the operation. This would allow our codewords to contain higher Fock states. Importantly, the SNAPPA gates can be scaled by adding additional drives without a significant overhead in calibration or significant degradation of fidelity. In [20], we present a calibration procedure that adds small overhead when adding additional drives. We demonstrate the case of three simultaneous drives to the cavity where we have added a drive for the transition $|5\rangle|g\rangle \rightarrow |6\rangle|e\rangle$. We prepare $(|1\rangle + |3\rangle + |5\rangle)|g\rangle/\sqrt{3}$ shown in figure 3(a). Qubit population and fidelity after state preparation are given by 0.05 and 0.92, respectively, shown in table 1. Applying the off-resonant drives, the qubit population becomes 0.90, meaning that the SNAPPA adds 0.05 error to the qubit population. We apply three cavity drives and one qubit drive. Now the phase of the second cavity drive at frequency $\omega_c + \Delta - 4\chi$ directly maps onto the phase of Fock state $|4\rangle$, and the phase of the third cavity drive at frequency $\omega_c + \Delta - 6\chi$ maps onto the phase of Fock state $|6\rangle$. Phases of the qubit drive and the first cavity drive at frequency $\omega_c + \Delta - 2\chi$ are always kept at 0 as reference. We show four states in figures 3(b)–(d), namely $(1/\sqrt{3})(|2\rangle + |4\rangle e^{i\theta_{3\rightarrow 4}} + |6\rangle e^{i\theta_{5\rightarrow 6}})|e\rangle$, where $(\theta_{3\rightarrow 4}, \theta_{5\rightarrow 6})$ is equal to $(0,0), (\pi,0)$, $(0,\pi)$ and (π,π) respectively. The state fidelity is equal for all four states (0.93) and the error introduced by the SNAPPA gate to the qubit state population is 0.05. This is similar to the errors introduced by the SNAPPA gate in figure 2 that is driving one less transition.

In this work, we demonstrate SNAPPA gates involving up to three simultaneous photon transitions. Scaling to higher photon numbers introduces technical challenges. A primary limitation is the complexity of calibrating multi-tone control pulses, which grows with the number of tones. The calibration procedure used in this work (for more details, see [20]) is recursive and local: we add one drive at a time and iteratively recalibrate earlier ones, which makes it difficult to guarantee globally optimal parameters as the number of transitions increases. To address this, more recently, some of us have developed a theoretical model [21] that accurately captures the dynamics of SNAPPA gates, enabling more systematic and efficient optimization of multitone drives. This model can be used in future work to streamline calibration and extend the protocol to higher Fock states more efficiently. In addition, as the system scales, higher-order nonlinearities intrinsic to the qubit-cavity interaction may become more prominent and must be carefully managed to maintain gate fidelity [3, 6].

In figure 4 we demonstrate one more application of the SNAPPA gate. One can drive transitions for *all* photon numbers n smaller than a maximum number to implement deterministic photon addition [15]. This operation is a sibling to the probabilistic photon creation operator a^{\dagger} often referred to as 'single-photon addition' in quantum optics [16]. As an example, we apply the SNAPPA gate $S_{PA}(0_{0\rightarrow 1}, 0_{1\rightarrow 2})$ by drives $|0\rangle|g\rangle \rightarrow |1\rangle|e\rangle$ and $|1\rangle|g\rangle \rightarrow |2\rangle|e\rangle$ on the initial state $(|0\rangle + |1\rangle e^{i\pi})|g\rangle/\sqrt{2}$ shown in figure 4(a) with qubit population 0.02 and cavity state fidelity 0.93 in table 1. Thus, the cavity state becomes $(|1\rangle + |2\rangle e^{i\pi})/\sqrt{2}$

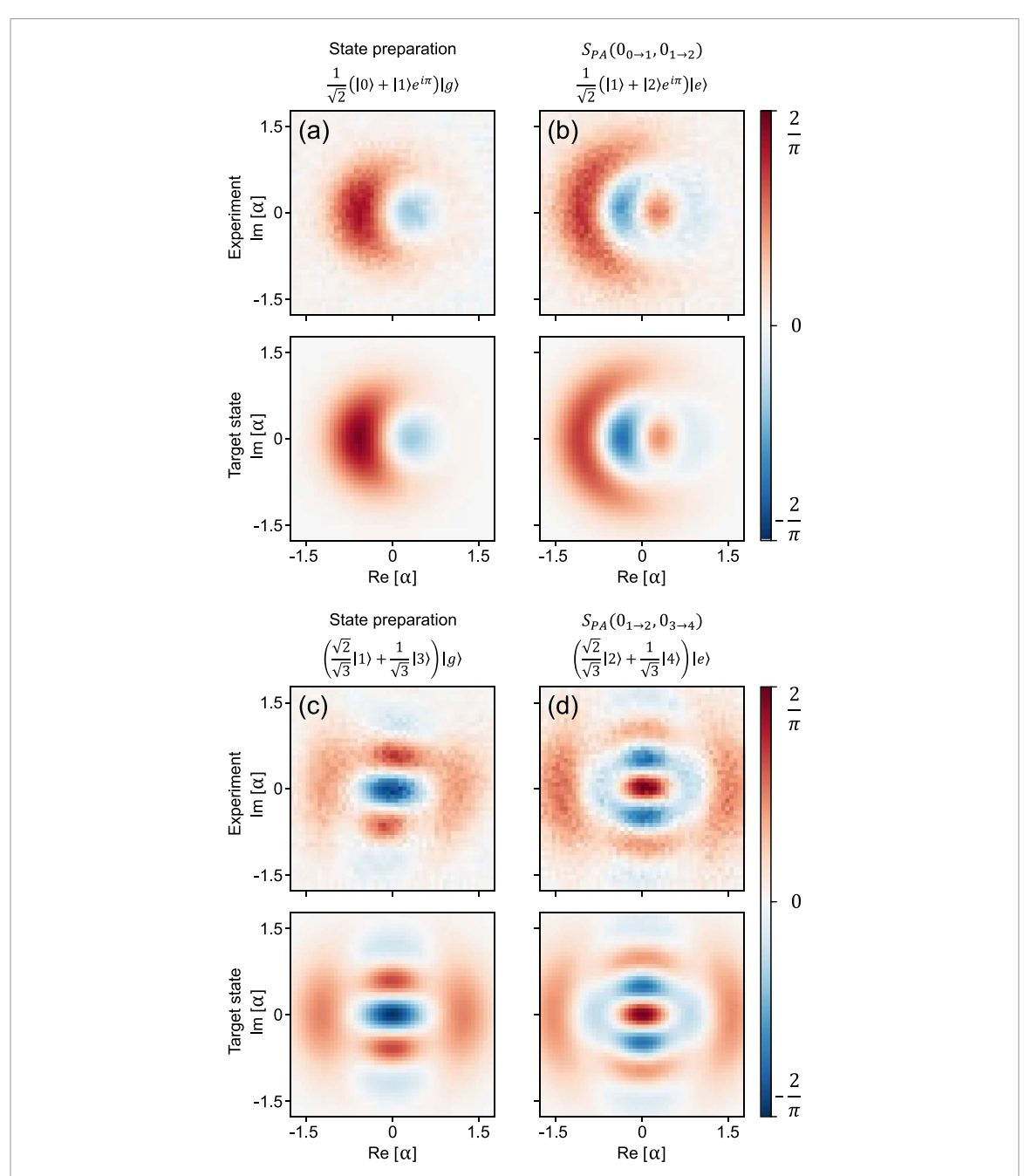


Figure 4. Wigner functions of experimental and target states. (a) Initial state $(|0\rangle + |1\rangle e^{i\pi})|g\rangle/\sqrt{2}$ and $(b)|1\rangle + |2\rangle e^{i\pi})|e\rangle/\sqrt{2}$, when drives $|0\rangle|g\rangle \rightarrow |1\rangle|e\rangle$ and $|1\rangle|g\rangle \rightarrow |2\rangle|e\rangle$ are applied. (c) Initial state $(\sqrt{2}/\sqrt{3}|1\rangle + 1/\sqrt{3}|3\rangle)|g\rangle$ and (d) state $(\sqrt{2}/\sqrt{3}|2\rangle + 1/\sqrt{3}|4\rangle)|e\rangle$, when drives $|1\rangle|g\rangle \rightarrow |2\rangle|e\rangle$ and $|3\rangle|g\rangle \rightarrow |4\rangle|e\rangle$ are applied.

(figure 4(b)), with the qubit population 0.94 and the state fidelity 0.92 (table 1). Another example is shown in figures 4(c) and (d) for unequal superpositions of the two Fock states. Preparing the cavity in the state $\left(\sqrt{2}/\sqrt{3}\right)|1\rangle+\left(1/\sqrt{3}\right)|3\rangle$ (figure 4(c)), we apply the same drives as in the case of figure 2(b) to create $\left(\sqrt{2}/\sqrt{3}\right)|2\rangle+\left(1/\sqrt{3}\right)|4\rangle$ (figure 4(d)) with qubit population 0.91 and state fidelity 0.96 (table 1).

4. Discussion

By using off-resonant drives, we have demonstrated the ability to selectively climb the Fock ladder and add arbitrary phases to the Fock states whose number is increased. Multiple such operations can be performed simultaneously. Similar to SNAP gates, SNAPPA gates need to be much longer than the inverse of the dispersive shift between the qubit and the cavity ($t_{\text{SNAPPA}} \gg 1/\chi$). However, it is likely possible to optimize the envelope shapes of off-resonant drives in order to shorten the gate time, as demonstrated for SNAP gates [4]. Furthermore, using the third level of the qubit, SNAP gates were made path independent [24, 25] which could possibly be adapted to make SNAPPA gates path independent as well. It is also straightforward

to implement a gate that selectively subtracts a photon while adding an arbitrary phase and exciting the qubit, as in the transformation $|n+1\rangle|g\rangle \to \mathrm{e}^{\mathrm{i}\theta_n}|n\rangle|e\rangle$. To drive this transition, we need drives whose frequencies satisfy $\omega_{qs}-\omega_{cs}=\omega_q-\omega_c-n\chi$. Keeping the qubit off-resonant drive the same, as in the case of SNAPPA gates ($\omega_q-\Delta$), we should further apply n cavity off-resonant drives at frequencies $\omega_c-\Delta+n\chi$ to implement SNAP photon subtraction. These drives can be combined with SNAPPA drives to give more functionality.

In our protocol, the SNAPPA drives are designed to selectively convert odd-parity states into even-parity states while leaving even-parity states unaffected. Regardless of the initial state's parity, the combined effects of the Stark shift and Kerr nonlinearity result in a rotation of the Wigner function. For odd-parity states, we compensate for this rotation by optimizing the phases of the SNAPPA drives, which selectively target the odd-parity states. In contrast, for even-parity states, no compensation is done, as the SNAPPA drives are intentionally configured to avoid interaction with these states, thereby maintaining the selective nature of our protocol. Importantly, in the context of error correction, we have the flexibility to choose the reference phase. This allows us to align the phase of the corrected state with the phase it would have acquired deterministically in the absence of errors. Consequently, the error correction process ensures that the final state retains the expected phase, effectively mitigating any unwanted phase deviations. However, this argument is valid when considering a superposition of only two Fock states, as in figure 2, where the Kerr effect simply introduces a global phase that can be factored out while preserving the relative phase between the states. For larger superpositions, such as in figure 3, the Kerr effect leads to different phases on each Fock component. In the case of odd-to-even parity transitions, SNAPPA corrects the phases on odd states caused by Kerr, since we are actively addressing the odd-parity states. For even-parity states, however, the Kerr effect cannot be corrected by a simple rotation of the reference frame. Instead, it could be mitigated by applying a selective SNAP gate, as SNAP gates are specifically designed to apply phase corrections to individual Fock states.

To further improve SNAPPA, several aspects could be explored. First, improving the qubit lifetime would significantly enhance the fidelity of the gate [11]. Second, optimizing the pulse shapes and parameters to minimize qubit-induced errors, such as relaxation, dephasing, and leakage, could enhance the fidelity of the gate. Third, developing techniques that decouple the qubit from the cavity more efficiently after the gate operation could mitigate transmon-induced decoherence in subsequent steps. Additionally, implementing an active or passive qubit reset immediately after the SNAPPA gate would prevent qubit population errors from propagating into the Wigner tomography. More generally, alternative state-reconstruction methods that do not rely on direct qubit involvement, such as using auxiliary qubits for indirect measurement [26, 27], could further reduce errors and are an important direction for future work.

A more precise characterization of the SNAPPA gate fidelity could, in principle, be obtained by applying the gate multiple times to amplify errors. While such an approach is not implemented in this work, we highlight it as a promising direction for future experiments aiming to study and benchmark gate performance more thoroughly.

The error recovery map probably could also be realized by using gradient-based optimization protocols such as GRAPE [5, 6, 28]. However, such black-box optimization will likely be very sensitive to system parameter calibration (including detailed stark shifts depending on precise driveline transmittance). In contrast, SNAPPA provides an interpretable calibration procedure.

In principle, the SNAPPA gate presented in equation (1) could be decomposed into a sequence of displacement and SNAP gates or via full optimal control such as GRAPE. However, in this work, we focus on the direct implementation of the exact recovery map in equation (1), using the control drives and approach outlined in this paper and leave a detailed comparison for future work. We limit our comparison to noting, (i) incorporating displacement gates into the unitary process likely leads to temporary population of higher Fock states, which might make the protocol more susceptible to noise, (ii) GRAPE-based optimization might be very sensitive to parameter calibration in contrast to our implementation of SNAPPA where the gate is tuned up in a systematic iterative way.

In the context of quantum error correction, the SNAPPA drives can autonomously detect and correct changes in the parity of an initial superposition of Fock states, due to single-photon loss. To complete the error correction cycle, qubit reset must be performed. Importantly, since the reset operation in our protocol does not need to be photon-number dependent, it can be implemented using established techniques for unconditional reset, such as all-microwave protocols [29] or active reset via measurement and feedback [30]. These methods allow for fast and efficient reinitialization of the ancillary qubit without disturbing the cavity state. Depending on the desired architecture, the reset can be applied either continuously, using autonomous schemes with additional drive tones [13], or in a pulsed manner, alternating photon addition and qubit reset. These strategies are well established and compatible with our proposed SNAPPA-based gates. More generally, SNAPPA gates make it possible to realize a family of non-unitary operations on the cavity, assisted by the

ancillary qubit. These operations may be useful in the context of quantum algorithms to implement block encodings [31].

Data availability statement

All data that support the findings of this study are included within the article (and any supplementary files).

Acknowledgments

We would like to thank Mats Myremark and Lars Jönsson for machining the cavity. SG would like to thank Matteo Lostaglio for the useful discussions. AME would like to thank Giulia Ferrini for the useful discussions. The simulations and visualization of the quantum states were performed using QuTiP [32, 33], NumPy [34], and Matplotlib [35]. The automatic differentiation tools TensorFlow [36] and Jax [37] were used in state reconstruction and optimization. This work was supported by the Knut and Alice Wallenberg Foundation via the Wallenberg Centre for Quantum Technology (WACQT) and by the Swedish Research Council. The chips were fabricated in the Chalmers Myfab cleanroom.

ORCID iDs

Marina Kudra © 0000-0003-4593-2859
Martin Jirlow © 0009-0000-0160-4787
Mikael Kervinen © 0000-0002-0164-9173
Axel M Eriksson © 0000-0002-2757-9804
Fernando Quijandría © 0000-0002-2355-0449
Per Delsing © 0000-0002-1222-3506
Tahereh Abad © 0000-0002-6277-3477
Simone Gasparinetti © 0000-0002-7238-693X

References

- [1] Joshi A, Noh K and Gao Y Y 2021 Quantum information processing with bosonic qubits in circuit QED *Quantum Sci. Technol.* 6 033001
- [2] Heeres R W, Vlastakis B, Holland E, Krastanov S, Albert V V, Frunzio L, Jiang L and Schoelkopf R J 2015 Cavity state manipulation using photon-number selective phase gates *Phys. Rev. Lett.* 115 137002
- [3] Krastanov S, Albert V V, Shen C, Zou C-L, Heeres R W, Vlastakis B, Schoelkopf R J and Jiang L 2015 Universal control of an oscillator with dispersive coupling to a qubit *Phys. Rev. A* **92** 040303
- [4] Kudra M et al 2022 Robust preparation of wigner-negative states with optimized snap-displacement sequences PRX Quantum 3 030301
- [5] Eickbusch A, Sivak V, Ding A Z, Elder S S, Jha S R, Venkatraman J, Royer B, Girvin S, Schoelkopf R J and Devoret M H 2022 Fast universal control of an oscillator with weak dispersive coupling to a qubit *Nat. Phys.* 18 1464–9
- [6] Heeres R W, Reinhold P, Ofek N, Frunzio L, Jiang L, Devoret M H and Schoelkopf R J 2017 Implementing a universal gate set on a logical qubit encoded in an oscillator *Nat. Commun.* 8 94
- [7] Cai W, Ma Y, Wang W, Zou C-L and Sun L 2021 Bosonic quantum error correction codes in superconducting quantum circuits Fundam. Res. 1 50
- [8] Mirrahimi M, Leghtas Z, Albert V V, Touzard S, Schoelkopf R J, Jiang L and Devoret M H 2014 Dynamically protected cat-qubits: a new paradigm for universal quantum computation *New J. Phys.* 16 045014
- [9] Grimsmo A L, Combes J and Baragiola B Q 2020 Quantum computing with rotation-symmetric bosonic codes Phys. Rev. X 10 011058
- [10] Ofek N et al 2016 Extending the lifetime of a quantum bit with error correction in superconducting circuits Nature 536 441
- [11] Ni Z et al 2022 Beating the break-even point with a discrete-variable-encoded logical qubit (arXiv:2211.09319)
- [12] Hu L et al 2019 Quantum error correction and universal gate set operation on a binomial bosonic logical qubit Nat. Phys. 15 503
- [13] Gertler J M, Baker B, Li J, Shirol S, Koch J and Wang C 2021 Protecting a bosonic qubit with autonomous quantum error correction Nature 590 243
- [14] Campagne-Ibarcq P et al 2017 Deterministic remote entanglement of superconducting circuits through microwave two-photon transitions Phys. Rev. Lett. 120 200501
- [15] Um M, Zhang J, Lv D, Lu Y, An S, Zhang J-N, Nha H, Kim M S and Kim K 2016 Phonon arithmetic in a trapped ion system Nat. Commun. 7 11410
- [16] Parigi V, Zavatta A, Kim M and Bellini M 2007 Probing quantum commutation rules by addition and subtraction of single photons to/from a light field *Science* 317 1890
- [17] Reagor M et al 2016 Quantum memory with millisecond coherence in circuit QED Phys. Rev. B 94 014506
- [18] Kudra M, Biznárová J, Fadavi Roudsari A, Burnett J J, Niepce D, Gasparinetti S, Wickman B and Delsing P 2020 High quality three-dimensional aluminum microwave cavities Appl. Phys. Lett. 117 070601
- [19] Tholén M O et al 2022 Measurement and control of a superconducting quantum processor with a fully integrated radio-frequency system on a chip Rev. Sci. Instrum. 93 104711
- [20] Supplementary material
- [21] Jirlow M, Helambe K, Eriksson A M, Gasparinetti S and Abad T 2025 Effective Hamiltonian for an off-resonantly driven qubit-cavity system (arXiv:2509.03375)

- [22] Ahmed S, Sánchez Mu noz C, Nori F and Kockum A F 2021 Quantum state tomography with conditional generative adversarial networks Phys. Rev. Lett. 127 140502
- [23] Ahmed S, Sánchez Mu noz C, Nori F and Kockum A F 2021 Classification and reconstruction of optical quantum states with deep neural networks Phys. Rev. Res. 3 033278
- [24] Reinhold P, Rosenblum S, Ma W-L, Frunzio L, Jiang L and Schoelkopf R J 2020 Error-corrected gates on an encoded qubit Nat. Phys. 16 822
- [25] Ma W-L, Zhang M, Wong Y, Noh K, Rosenblum S, Reinhold P, Schoelkopf R J and Jiang L 2020 Path-independent quantum gates with noisy ancilla Phys. Rev. Lett. 125 110503
- [26] da Silva M P, Taylor J M and Lukin M D 2009 Quantum state tomography via quantum circuits Phys. Rev. A 79 052320
- [27] Gomes R M, de Matos Filho R L and Huguenin J A O 2016 Quantum metrology with auxiliary qubits Phys. Rev. A 93 052118
- [28] Puviani M, Borah S, Zen R, Olle J and Marquardt F 2025 Non-Markovian feedback for optimized quantum error correction Phys. Rev. Lett. 134 020601
- [29] Magnard P et al 2018 Fast and unconditional all-microwave reset of a superconducting qubit Phys. Rev. Lett. 121 060502
- [30] Ristè D, Bultink C C, Lehnert K W and DiCarlo L 2012 Feedback control of a solid-state qubit using High-fidelity projective measurement Phys. Rev. Lett. 109 240502
- [31] Rall P 2020 Quantum algorithms for estimating physical quantities using block encodings Phys. Rev. A 102 022408
- [32] Johansson J R, Nation P D and Nori F 2012 QuTiP: an open-source Python framework for the dynamics of open quantum systems Comput. Phys. Commun. 183 1760
- [33] Johansson J R, Nation P D and Nori F 2013 QuTiP 2: a Python framework for the dynamics of open quantum systems Comput. Phys. Commun. 184 1234
- [34] Harris C R et al 2020 Array programming with NumPy Nature 585 357
- [35] Hunter J D 2007 Matplotlib: a 2d graphics environment Comput. Sci. Eng. 9 90
- [36] Abadi M *et al* 2015 TensorFlow: large-scale machine learning on heterogeneous systems (software available from tensorflow.org) (available at: www.tensorflow.org/)
- [37] Bradbury J et al 2018 JAX: composable transformations of Python+NumPy programs (available at: http://github.com/google/jax)